Publisher: GSA
Journal: GEOL: Geology
DOI:10.1130/G37490.1

Age of the Laschamp excursion determined by U-Th dating of a speleothem geomagnetic record from North America

Ioan Lascu[1,2,3*], Joshua M. Feinberg[1,2], Jeffrey A. Dorale[4], Hai Cheng[2,5], and R. Lawrence Edwards[2]

[1]*Institute for Rock Magnetism, University of Minnesota, 100 Union Street SE, Minneapolis, Minnesota 55455, USA*

[2]*Department of Earth Sciences, University of Minnesota, 310 Pillsbury Drive SE, Minneapolis, Minnesota 55455, USA*

[3]*Department of Earth Sciences, University of Cambridge, Downing Street, Cambridge, CB2 3EQ, UK*

[4]*Department of Earth and Environmental Sciences, University of Iowa, 115 Trowbridge Hall, Iowa City, Iowa 52242, USA*

[5]*Institute of Global Environmental Change, Xi'an Jiaotong University, Xi'an 710049, China*

*E-mail: il261@cam.ac.uk

ABSTRACT

The Laschamp geomagnetic excursion was the first short-lived polarity event recognized and described in the paleomagnetic record, and to date remains the most studied geomagnetic event of its kind. In addition to its geophysical significance, the Laschamp is an important global geochronologic marker. The Laschamp excursion occurred around the time of the demise of *Homo neanderthalensis*, in conjunction with high-amplitude, rapid climatic oscillations leading into the Last Glacial Maximum, and coeval with a major supervolcano eruption in the Mediterranean. Thus, precise determination of the timing and duration of the Laschamp excursion would help in elucidating major scientific questions situated at the intersection of geology, paleoclimatology, and anthropology. Here we present a North American speleothem geomagnetic record of the Laschamp excursion that is directly dated using a combination of high-precision ^{230}Th dates and annual layer counting using confocal microscopy. We have determined a maximum excursion duration that spans the interval 42,250–39,700 yr BP, and an age of 41,100 ± 350 yr BP for the main phase of the excursion, during which the virtual geomagnetic pole was situated at the southernmost latitude in the record. Our chronology provides the first age bracketing of the Laschamp excursion using radioisotopic dating, and improves on previous age determinations based on ^{40}Ar/^{39}Ar dating of lava flows, and orbitally-tuned sedimentary and ice-core records.

INTRODUCTION

One of the frontiers of paleomagnetic research is focused on the understanding of the Earth's magnetic field behavior during geomagnetic excursions. Excursions are short-lived geomagnetic events during which the virtual geomagnetic pole (VGP) deviates by more than 45° from the normal range of secular variation (Merrill and McFadden, 1994), typically accompanied by a decrease in the strength of the geodynamo's dipolar field component (Laj and Channell, 2007). Information regarding the anatomy, timing, and duration of excursions can serve to calibrate magneto-hydrodynamic modeling of outer core flow dynamics on centennial to millennial scales, thus helping to understand the intrinsic behavior of Earth's dynamo (Gubbins, 1999). In addition, accurate and precise, high-resolution time series of geomagnetic excursions are critical for dating geologic phenomena, climatic episodes, astronomical events, or paleontologic and anthropologic stratigraphic markers (Leonhardt et al., 2009; Richards and Andersen, 2013; Singer, 2014).

The Laschamp excursion is the first geomagnetic excursion described in the paleomagnetic record, and remains the most studied geomagnetic event of its kind to date (Laj and Channell, 2007, and references therein). Current estimates of the age of the Laschamp, based on radioisotopic dating of volcanic rocks, place the excursion at ~41 ka BP (40.70 ± 0.95 ka BP according to Singer et al., 2009, and 41.30 ± 0.60 ka BP according to Laj et al., 2014). In parallel, developments in sediment geochronology and paleomagnetism have enabled the reconstruction of past field behavior during the Laschamp at very high resolution in sediment cores, placing constraints on the total extent of the excursion to <3,000 years (e.g., Lund et al., 2005; Muscheler et al., 2005; Channell, 2006; Laj et al., 2006; Ménabréaz et al., 2011), and on its main phase to <1,000 years (e.g., Channell, 2006; Laj et al., 2006; Channell et al., 2012; Nowaczyk et al., 2012; Bourne et al., 2013; Laj et al., 2014). However, the timing of the Laschamp cannot be directly determined from the same sediment records in most cases. This pitfall often leads to tuning of geochemical proxies in the sedimentary records to those in ice core records, which in turn are tuned to astronomically-paced changes in Earth's orbital parameters—the so-called astrochronologic framework (Laj and Channell, 2007; Nowaczyk et al., 2012). This approach has some major caveats, as discussed by Blaauw (2012).

Speleothems (chemical sedimentary deposits formed in caves) hold certain key advantages for documenting geomagnetic excursions over traditional paleomagnetic archives (Lascu and Feinberg, 2011). They are crystalline, and therefore avoid

DOI:10.1130/G37490.1

complications associated with remanence acquisition in soft sediments. The time lag between the deposition of magnetic particles on speleothem surfaces and their encapsulation in the crystalline structure is short, as demonstrated by actively-growing stalagmites that record the magnetic direction of the ambient magnetic field (e.g., Latham et al., 1979; Morinaga et al., 1989). Speleothems may grow continuously for thousands of years, and can be dated with very high accuracy and precision using ^{230}Th dating, a technique that can be reliably used on specimens <600–700 ka in age (Edwards et al., 2003; Dorale et al., 2004, Cheng et al., 2013). Recent speleothem magnetism studies have shown that magnetic minerals encapsulated in stalagmites (e.g., Strauss et al., 2013; Font et al., 2014) can be used successfully in dating geomagnetic excursions (Osete et al., 2012), as well as for reconstructing hydrologic and climatic variations (Xie et al., 2013; Bourne et al., 2015). Here we present a speleothem geomagnetic record from Crevice Cave, Missouri (Dorale et al., 1998) that captures the changes in geomagnetic field direction and intensity associated with the Laschamp excursion, dated directly on speleothem calcite using a combination of high-precision ^{230}Th dating and incremental chronometry from annual growth laminae.

METHODS

Crevice Cave (37.75 N, 89.83 W) is Missouri's longest known cave at >45 km in length, and is situated close to the mid-continent tall grass prairie–deciduous forest ecotone, ~200 km from the southern maximum extent of the Laurentide ice sheet (Dorale et al., 1998). The studied speleothem was found in a naturally broken state, in a stream-level passage of the cave. Two parallel slabs, ~19 cm in length, were cut along the central axis of the speleothem, where growth laminae were horizontal. One of the slabs was sliced into ~0.5 cm specimens using a wire saw, and used for paleomagnetic and mineral magnetic analyses at the Institute for Rock Magnetism. Details of the experimental protocols can be found in the Data Repository. The other slab was used for constructing the age model. A Nikon A1R confocal microscope was used on the top 5 cm of the slab to image growth bands (Fig. DR1), based on the property of fluorescence of organic-rich layers when exposed to source light with wavelengths of 400–500 nm. Subsequently, calcite powders were collected for ^{234}U-^{230}Th dating from 10 horizons, each between 0.6 and 1 mm in thickness, by drilling with a dental burr parallel to the growth laminae. The locations of the third and fifth dating horizons from the top were chosen to bracket the Laschamp excursion as determined from the paleomagnetic measurements. The fourth dating horizon was chosen to correspond to the paleomagnetic specimen encompassing the maximum VGP latitude deviation. Uranium and thorium isotope ratios were measured on a Thermo Neptune multi-collector inductively coupled plasma–mass spectrometer at the University of Minnesota, following the methodology of Cheng et al. (2013). An incremental chronology was obtained by counting the annual layers from the confocal micrographs between the base of the fifth and top of the third dating horizons.

RESULTS

Chronology

The radioisotopic ages are all in stratigraphic order and are reported with 2σ uncertainties (Fig. 1 and Table DR1). The speleothem started forming during marine isotope stage 4 and stopped growing just prior to the last glacial maximum (LGM). Growth rates decreased from 7 to 8 mm/ka during the first part of the record to ~5 mm/ka around the time of the Laschamp, eventually reaching very low values (~1 mm/ka) in the final ~10 ka of the record (Fig. 1H). The age-depth curve was obtained by interpolating linearly between the ^{230}Th dates (Fig. 1F), except between 42,167 ± 101 and 39,179 ± 121 yr BP, where the incremental chronology (Fig. 1G), anchored to base of the fifth dating horizon, was used. We counted 2975 ± 20 laminae, which is in excellent agreement with the radioisotopic age difference of 2988 (with 2σ errors of ± ~100 years), confirming the annual nature of the calcite growth bands. The depth-age relationship is linear between the ^{230}Th dates of 42,167 ± 101 and 41,033 ± 132 yr BP, but deviates slightly from this trend between 41,033 ± 132 and 39,179 ± 121 yr BP, as growth slowed approaching the LGM.

Rock Magnetism and Paleomagnetism

The main magnetic carrier in our specimens is magnetite, as revealed by low temperature experiments (Fig. 2B). The ratio of anhysteretic remanent magnetization (ARM) susceptibility (χ_{ARM}) to isothermal remanent magnetization (IRM), or χ_{ARM}/IRM, a grain size indicator, is <0.4 mm/A for specimens older than ~55 ka BP, and >0.4 mm/A for younger specimens (Fig. 1D). Around 41 ka BP, χ_{ARM}/IRM is ~1 mm/A, a value typical for pedogenic single domain magnetite particles, a few tens of nm in size (Geiss et al., 2008). Lower values indicate a more important admixture of coarser, lithogenic magnetic grains.

Paleomagnetic directions exhibit a significant deviation from normal secular variation values between ~42 and ~39 ka BP, an event we associate with the Laschamp excursion (Fig. 1A-C, 1E). Inclination values decrease to ~10° shortly after 42.2 ± 0.1 ka BP (Fig. 1A), and the main declination swing occurs around 41.0 ± 0.1 ka BP (Fig. 1B), lagging the first inclination change by ~1 ka. The ratio of natural remanent magnetization

(NRM) to ARM, a relative paleointensity proxy, is lowest at ~41 ka (Fig. 1C), concomitant with the maximum directional excursion. The decrease in NRM/ARM is a change of one order of magnitude compared to average background values, and is not due to a magnetic grain size change, as χ_{ARM}/IRM remains fairly constant (Fig. 1D, 2A). The VGP lies in the southern hemisphere at this time (~–30°, Fig. 1E).

The alternating field (AF) demagnetization experiments generally show a (quasi-) linear decay of the NRM toward the origin (Fig. 2C-D, DR2) even for specimens with lower magnetic concentrations (NRM <10^{-7} Am^2/kg). Viscous overprints are removed at 2–5 mT peak AF demagnetization fields (Fig. 2C-E). Based on the demagnetization behavior of most of the specimens, we attribute clustering demagnetization patterns (e.g., Fig. 2E) to low intensity levels (NRM <10^{-8} Am^2/kg), rather than to erratic demagnetization behavior.

DISCUSSION

Timing and Duration of the Laschamp Excursion

Radioisotopic dating of volcanic rocks, mainly using the $^{40}Ar/^{39}Ar$ method, is the current state-of-the-art approach to determining the timing of Late Quaternary geomagnetic events (Singer, 2014). Recent Laschamp age determinations are reported by Singer et al. (2009) and Laj et al. (2014), who place the excursion at 40.70 ± 0.95 ka BP and 41.30 ± 0.60 ka BP, respectively. These age estimates, however, were determined by pooling data sets from various flows that yield individual ages with errors >1 ka in all cases. The $^{234}U/^{230}Th$ method applied to speleothems has the potential of providing individual errors at least an order of magnitude smaller for calcite precipitated ~40 ka ago (Cheng et al., 2013). The Crevice Cave specimen, albeit slow-growing, has rather high concentrations of uranium (Table DR1), which allows for ^{230}Th dates to be determined with errors of ~100 years for calcite horizons <1 mm in thickness. Our paleomagnetic specimens are 4–5 mm thick, so after factoring in the sampling resolution, we find that the main phase of the Laschamp excursion in our speleothem occurred at 41.10 ± 0.35 ka BP, as determined from the specimen that contains the maximum VGP deviation (Fig. 1). This refines the precision of the excursion timing compared to the age estimates proposed by Singer et al. (2009) and Laj et al. (2014), with improved error estimates by a factor of 2–3. The uncertainty of the timing of the Laschamp excursion could be further refined using this approach by targeting speleothems with higher growth rates.

Although lava flows provide excellent spot records of geomagnetic excursions, the current dating precision of the ^{40}Ar/^{39}Ar method is on the order of several ka, precluding any meaningful attempt at robustly bracketing the duration of such short-lived events. The two ^{230}Th dates bracketing the Laschamp excursion in the Crevice Cave speleothem serve as anchors to an incremental age model that allows the calculation of the time interval covered by the speleothem specimens that contain the field directional swing and intensity low that define the excursion. According to our speleothem record, the entire excursion spans the time interval from 42.25 ka BP to 39.70 ka BP, for a duration of ~2,550 years. The main phase of the Laschamp is defined by one speleothem specimen, which encompasses ~700 years for which the field direction was of reverse polarity (average VGP latitude of around -30°). These are maximum values, and are consistent with excursion durations determined from sedimentary records around the globe. One of the best records of the Laschamp excursion comes from the Black Sea, where the entire period of directional variations was estimated to be just under 3,000 years, with transitional or reverse directions (and associated paleointensity low) lasting ~1,600 years, out of which fully reverse directions were maintained for 440 years (Nowaczyk et al., 2012). Similarly, a short full reversal of 0.4–0.8 ka, superimposed on a background of low relative paleointensity that lasted 1.5–2 ka is reported from cores from the Blake Ridge (Bourne et al., 2013), Bermuda Rise (Kissel et al., 1999; Channell et al., 2012), Irminger Basin (Channell, 2006), NW of Iceland and Southern Indian Ocean (Laj et al., 2006). These paleomagnetic data are consistent with cosmogenic nuclide production rates from sediment and ice cores (e.g., Muscheler et al., 2005; Ménabréaz et al., 2011; Nilsson et al., 2011), and are supported by Bayesian inversion of geomagnetic field evolution during the Laschamp in North America (Leonhardt et al., 2009). Bayesian inversion also suggests that the timing and duration of the Laschamp may vary according to locality (Leonhardt et al., 2009). Precise dating of additional speleothem geomagnetic records of the Laschamp from key locations around the globe would provide the means for testing this inferred asynchroneity.

Potential of Speleothems in Dating Brunhes-Age Excursions

Geomagnetic excursions are reflections of geodynamo dynamics on short time scales. A rigorous documentation of the anatomy, timing, duration, and/or frequency of such short-lived events can be invaluable for theoretical and numerical geodynamo models. Well-constrained age models are critical for characterizing geomagnetic instabilities, and are key in developing high-resolution geomagnetic time series. One such effort is the development of the Quaternary geomagnetic instability time scale (GITS). Within this framework, Singer (2014) has synthesized the current understanding of excursional occurrence within the Brunhes chron. Geomagnetic excursions appear to be concentrated within two ~200 ka time periods (722–528 ka BP and 211–17 ka BP), each containing half a dozen excursions, that are in the dating range of the $^{234}U/^{230}Th$ method (Edwards et al., 2003; Dorale et al., 2004, Cheng et al., 2013). The younger Brunhes excursions would particularly benefit from precise pinpointing by taking advantage of this method, which under ideal circumstances yields 2σ uncertainties as low as ± 0.1 ka at 130 ka BP, and ± 0.3 ka at 200 ka BP (Cheng et al., 2013). The older Brunhes excursions, although pushing the limit of the ^{230}Th dating method (2σ uncertainties of ± 6 ka at 500 ka BP and ± 12 ka at 600 ka BP), could also benefit from this approach, especially if there is a possibility to combine radioisotopic and incremental dating methods. Cheng et al. (2013) provide a good example of dating a speleothem that formed between 640 and 510 ka BP, demonstrating the viability of the $^{234}U/^{230}Th$ method.

ACKNOWLEDGMENTS

This project was funded by NSF-EAR grant 1316385, a University of Minnesota McKnight Land Grant Professorship to JMF, and ERC grant 320750. Confocal microscopy was performed at the University of Minnesota Imaging Centers. We are grateful to John Geissman, Brad Singer, and James Channell for their constructive reviews. This is Institute for Rock Magnetism contribution 1506.

REFERENCES CITED

Blaauw, M., 2012, Out of tune: The dangers of aligning proxy archives: Quaternary Science Reviews, v. 36, p. 38–49, doi:10.1016/j.quascirev.2010.11.012.

Bourne, M.D., Mac Niocaill, C., Thomas, A.L., and Henderson, G.M., 2013, High-resolution record of the Laschamp geomagnetic excursion at the Blake-Bahama

Outer Ridge: Geophysical Journal International, v. 195, p. 1519–1533, doi:10.1093/gji/ggt327.

Bourne, M.D., Feinberg, J.M., Strauss, B.E., Hardt, B., Cheng, H., Rowe, H.D., Springer, G., and Edwards, R.L., 2015, Long-term changes in precipitation recorded by magnetic minerals in speleothems: Geology, v. 43, p. 595–598, doi:10.1130/G36695.1.

Channell, J., 2006, Late Brunhes polarity excursions (Mono Lake, Laschamp, Iceland Basin and Pringle Falls) recorded at ODP Site 919 (Irminger Basin): Earth and Planetary Science Letters, v. 244, p. 378–393, doi:10.1016/j.epsl.2006.01.021.

Channell, J.E.T., Hodell, D.A., and Curtis, J.H., 2012, ODP Site 1063 (Bermuda Rise) revisited: Oxygen isotopes, excursions and paleointensity in the Brunhes Chron: Geochemistry Geophysics Geosystems, v. 13, Q02001, doi:10.1029/2011GC003897.

Cheng, H., Edwards, R.L., Shen, C.C., Polyak, V.J., Asmerom, Y., Woodhead, J., Hellstrom, J., Wang, Y., Kong, X., Spötl, C., Wang, X., and Alexander, E.C., 2013, Improvements in ^{230}Th dating, ^{230}Th and ^{234}U half-life values, and U-Th isotopic measurements by multi-collector inductively coupled plasma mass spectrometry: Earth and Planetary Science Letters, v. 371–372, p. 82–91, doi:10.1016/j.epsl.2013.04.006.

Dorale, J.A., Edwards, R.L., Ito, E., and González, L.A., 1998, Climate and Vegetation History of the Midcontinent from 75 to 25 ka: A Speleothem Record from Crevice Cave, Missouri, USA: Science, v. 282, p. 1871–1874, doi:10.1126/science.282.5395.1871.

Dorale, J.A., Edwards, R.L., Alexander, E.C., Shen, C., Richards, D.A., and Cheng, H., 2004, Uranium-series dating of speleothems: Current techniques, limits, & applications, *in* Sasowsky, I.D. and Mylroie, J.E., eds., Studies of Cave Sediments: Physical and Chemical Records of Paleoclimate: Netherlands, Springer, p. 177–197, doi:10.1007/978-1-4419-9118-8_10.

Edwards, R.L., Gallup, C.D., and Cheng, H., 2003, Uranium-series dating of marine and lacustrine carbonates, *in* Bourdon, B., Henderson, G.M., Lundstrom, C.C., and Turner, S.P., eds., Reviews in Mineralogy and Geochemistry: Uranium-Series Geochemistry: Washington, DC, Mineralogical Society of America, p. 363–405, doi:10.2113/0520363.

Font, E., Veiga-Pires, C., Pozo, M., Carvallo, C., de Siqueira Neto, A.C., Camps, P., Fabre, S., and Mirão, J., 2014, Magnetic fingerprint of southern Portuguese speleothems and implications for paleomagnetism and environmental magnetism: Journal of Geophysical Research, v. 119, p. 1–28, doi:10.1002/2014JB011381.

Geiss, C.E., Egli, R., and Zanner, C.W., 2008, Direct estimates of pedogenic magnetite as a tool to reconstruct past climates from buried soils: Journal of Geophysical Research, v. 113, no. B11, p. B11102, doi: 10.1029/2008JB005669.

Gubbins, D., 1999, The distinction between geomagnetic excursions and reversals: Geophysical Journal International, v. 137, p. F1–F4, doi:10.1046/j.1365-246x.1999.00810.x.

Kissel, C., Laj, C., Labeyrie, L., Dokken, T., Voelker, A., and Blamart, D., 1999, Rapid climatic variations during marine isotopic stage 3: Magnetic analysis of sediments from Nordic Seas and North Atlantic: Earth and Planetary Science Letters, v. 171, p. 489–502, doi:10.1016/S0012-821X(99)00162-4.

Laj, C., and Channell, J.E.T., 2007, Geomagnetic Excursions: Treatise on Geophysics, v. 5, p. 373–416, doi:10.1016/B978-044452748-6/00095-X.

Laj, C., Kissel, C., and Roberts, A.P., 2006, Geomagnetic field behavior during the Iceland Basin and Laschamp geomagnetic excursions: A simple transitional field geometry?: Geochemistry Geophysics Geosystems, v. 7, p. Q03004, doi:10.1029/2005GC001122.

Laj, C., Guillou, H., and Kissel, C., 2014, Dynamics of the earth magnetic field in the 10–75 kyr period comprising the Laschamp and Mono Lake excursions: New results from the French Chaîne des Puys in a global perspective: Earth and Planetary Science Letters, v. 387, p. 184–197, doi:10.1016/j.epsl.2013.11.031.

Lascu, I., and Feinberg, J.M., 2011, Speleothem magnetism: Quaternary Science Reviews, v. 30, p. 3306–3320, doi:10.1016/j.quascirev.2011.08.004.

Latham, A.G., Schwarz, H.P., Ford, D.C., and Pearce, G.W., 1979, Palaeomagnetism of stalagmite deposits: Nature, v. 280, p. 383–385, doi:10.1038/280383a0.

Leonhardt, R., Fabian, K., Winklhofer, M., Ferk, A., Laj, C., and Kissel, C., 2009, Geomagnetic field evolution during the Laschamp excursion: Earth and Planetary Science Letters, v. 278, p. 87–95, doi:10.1016/j.epsl.2008.11.028.

Lund, S.P., Scwartz, M., Keigwin, L., and Johnson, T., 2005, Deep-sea sediment records of the Laschamp geomagnetic field excursion (~41,000 calendar years before present): Journal of Geophysical Research, v. 110, B04101, doi:10.1029/2003JB002943.

Ménabréaz, L., Thouveny, N., Bourlès, D.L., Deschamps, P., Hamelin, B., and Demory, F., 2011, The Laschamp geomagnetic dipole low expressed as a cosmogenic ^{10}Be atmospheric overproduction at ~41ka: Earth and Planetary Science Letters, v. 312, p. 305–317, doi:10.1016/j.epsl.2011.10.037.

Merrill, R.T., and McFadden, P.L., 1994, Geomagnetic field stability: Reversal events and excursions: Earth and Planetary Science Letters, v. 121, p. 57–69, doi:10.1016/0012-821X(94)90031-0.

<jrn>Morinaga, H., Inokuchi, H., and Yaskawa, K., 1989, Palaeomagnetism of stalagmites (speleothems) in SW Japan: Geophysical Journal, v. 96, p. 519–528, doi:10.1111/j.1365-246X.1989.tb06011.x.</jrn>

Muscheler, R., Beer, J., Kubik, P.W., and Synal, H.-A., 2005, Geomagnetic field intensity during the last 60,000 years based on ^{10}Be and ^{36}Cl from the Summit ice cores and ^{14}C: Quaternary Science Reviews, v. 24, p. 1849–1860, doi:10.1016/j.quascirev.2005.01.012.

Nilsson, A., Muscheler, R., Snowball, I., Aldahan, A., Possnert, G., Augustinus, P., Atkin, D., and Stephens, T., 2011, Multi-proxy identification of the Laschamp geomagnetic field excursion in Lake Pupuke, New Zealand: Earth and Planetary Science Letters, v. 311, p. 155–164, doi:10.1016/j.epsl.2011.08.050.

Nowaczyk, N.R., Arz, H.W., Frank, U., Kind, J., and Plessen, B., 2012, Dynamics of the Laschamp geomagnetic excursion from Black Sea sediments: Earth and Planetary Science Letters, v. 351–352, p. 54–69, doi:10.1016/j.epsl.2012.06.050.

Osete, M.-L., Martín-Chivelet, J., Rossi, C., Edwards, R.L., Egli, R., Muñoz-García, M.B., Wang, X., Pavón-Carrasco, F.J., and Heller, F., 2012, The Blake geomagnetic excursion recorded in a radiometrically dated speleothem: Earth and Planetary Science Letters, v. 353–354, p. 173–181, doi:10.1016/j.epsl.2012.07.041.

Richards, D.A., and Andersen, M.B., 2013, Time Constraints and Tie-Points in the Quaternary Period: Elements (Quebec), v. 9, p. 45–51, doi:10.2113/gselements.9.1.45.

Singer, B.S., 2014, A Quaternary geomagnetic instability time scale: Quaternary Geochronology, v. 21, p. 29–52, doi:10.1016/j.quageo.2013.10.003.

Singer, B.S., Guillou, H., Jicha, B.R., Laj, C., Kissel, C., Beard, B.L., and Johnson, C.M., 2009, $^{40}Ar/^{39}Ar$, K–Ar and $^{230}Th–^{238}U$ dating of the Laschamp excursion: A radioisotopic tie-point for ice core and climate chronologies: Earth and Planetary Science Letters, v. 286, p. 80–88, doi:10.1016/j.epsl.2009.06.030.

Strauss, B.E., Strehlau, J.H., Lascu, I., Dorale, J.A., Penn, R.L., and Feinberg, J.M., 2013, The origin of magnetic remanence in stalagmites: Observations from electron microscopy and rock magnetism: Geochemistry Geophysics Geosystems, v. 14, p. 5006–5025, doi:10.1002/2013GC004950.

Xie, S., Evershed, R.P., Huang, X., Zhu, Z., Pancost, R.D., Meyers, P.A., Gong, L., Hu, C., Huang, J., Zhang, S., Gu, Y., and Zhu, J., 2013, Concordant monsoon-driven postglacial hydrological changes in peat and stalagmite records and their impacts on prehistoric cultures in central China: Geology, v. 41, p. 827–830, doi:10.1130/G34318.1.

FIGURE CAPTIONS

Figure 1. Magnetic properties and chronology of the Laschamp excursion in the speleothem specimen studied from Crevice Cave, Missouri: A) Inclination; B) Declination; C) Relative paleointensity (NRM/ARM); D) Magnetic grain size (χ_{ARM}/IRM); E) Virtual geomagnetic pole (VGP) latitude; F) Age-depth model based on ^{230}Th dates; G) Incremental chronology (from confocal microscopy layer-counting) across the Laschamp, anchored to radioisotopic dates; and H) Speleothem growth rates from the radioisotopic (black) and incremental (grey) age models. Upper and lower limits for declination (dashed lines in B) were calculated by rotating the specimen from −10° (lower limit) to 30° (upper limit). VGP latitude uncertainty (interval delineated by continuous lines in E) was calculated via rotating the specimen through a 40° declination range (see Data Repository). The Laschamp excursion is defined by the three specimens with notable departures in inclination, declination and relative intensity from background values (shades of grey; the main phase of the Laschamp is represented with a darker grey). A close-up of the 3 specimens (G) shows their individual thickness and time period covered. Previous age determinations of 40.7 ± 1.0 (Singer et al., 2009) and 41.3 ± 0.6 ka BP (Laj et al., 2014) are shown for comparison.

Figure 2. A) Comparison of natural remanent magnetization (NRM), anhysteretic remanent magnetization (ARM), and isothermal remanent magnetization (IRM) time series. Note deviation of NRM values from trends exhibited by ARM and IRM between 42 and 39 ka BP; B) Low temperature saturation IRM (LT-SIRM) behavior on warming after field-cooled (FC) and zero field-cooled (ZFC) pre-treatments, and room temperature saturation IRM (RT-SIRM) behavior on successive warming (black triangles) and

cooling (open triangles) cycles, showing the presence of oxidized magnetite; C-E) Orthogonal projections and azimuthal equidistant plots of specimens defining the Laschamp excursion (labeled on the NRM curve in A). Full (open) squares represent the horizontal (vertical) projections of the demagnetization vectors (grey arrows). Grey symbols are viscous overprints removed by AF peak fields of 5 mT. Unit in orthogonal plots is 5×10^{-12} Am^2. Magnetometer noise level is $\sim10^{-11}$ Am^2.

[1]GSA Data Repository item 2016xxx, xxxxxxxx, is available online at www.geosociety.org/pubs/ft2015.htm, or on request from editing@geosociety.org or Documents Secretary, GSA, P.O. Box 9140, Boulder, CO 80301, USA.

Figure1

LascuFig1

Click here to download Figure LascuFig1.eps

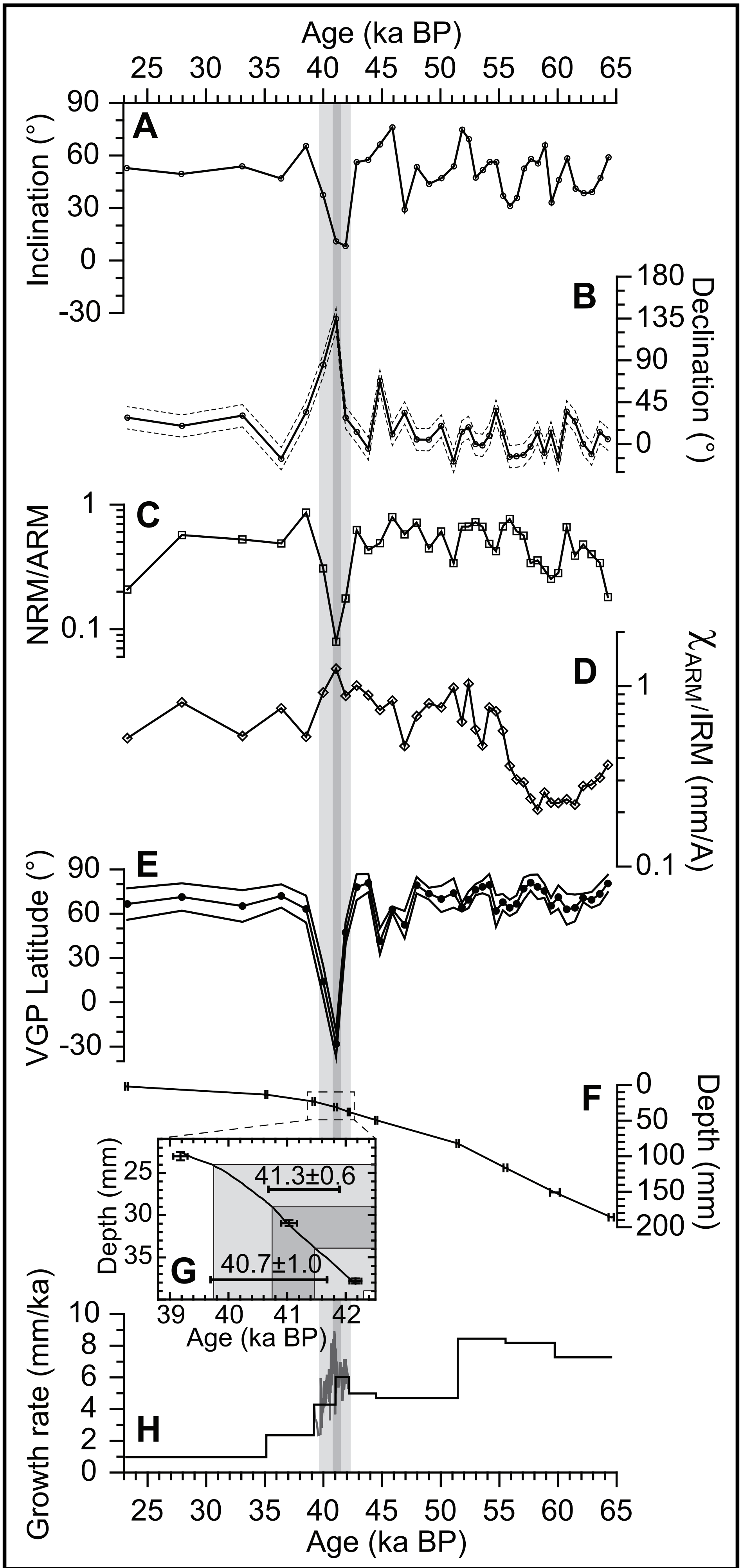

Figure2

Click here to download Figure LascuFig2.eps

LascuFig2

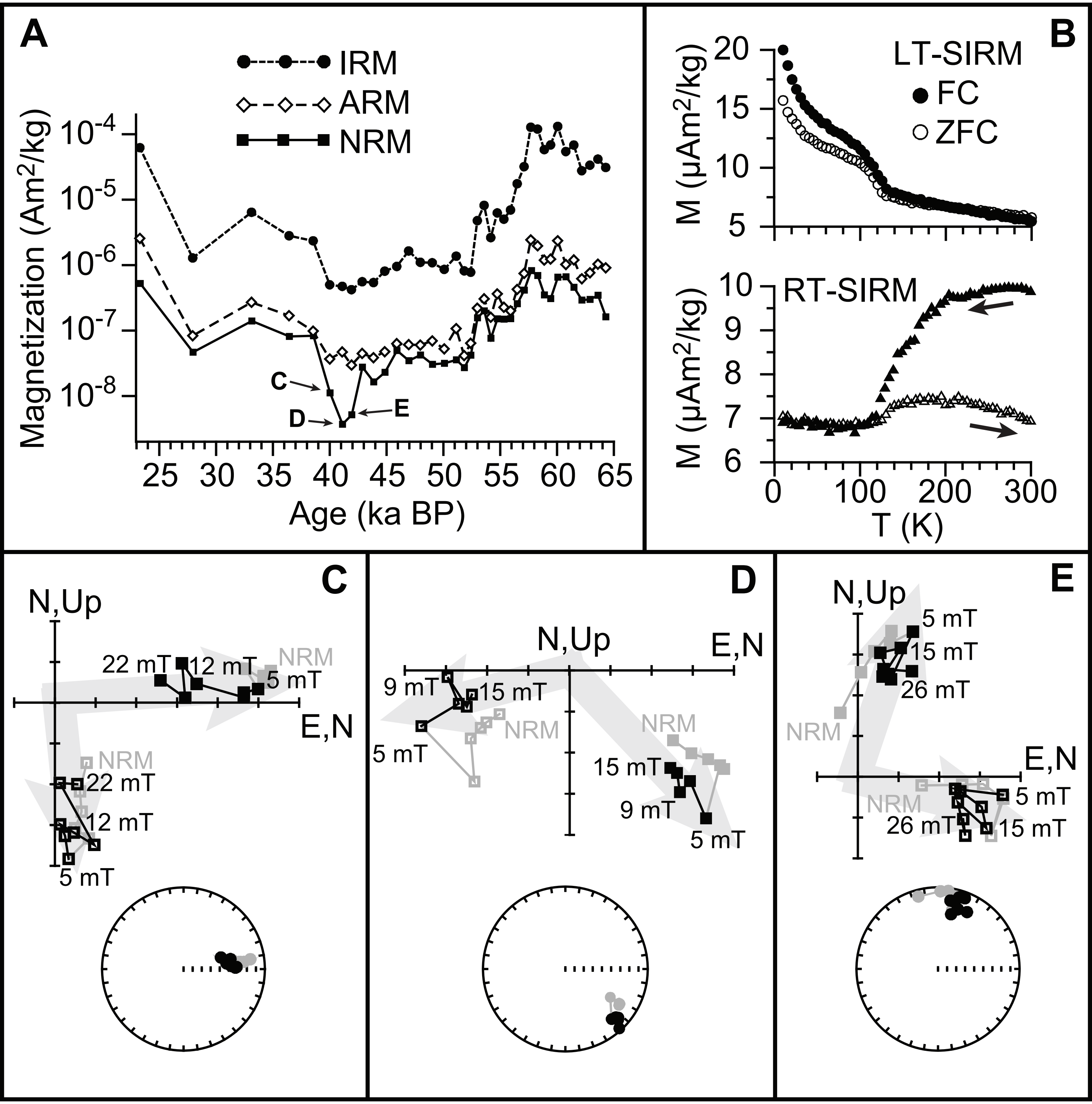

MAGNETIC METHODS

The slab used for paleomagnetism, with a cross section of 1.7 cm × 0.7 cm, was sectioned into 38 specimens, ~0.5 cm in thickness each. After measuring the natural remanent magnetization (NRM), each specimen was demagnetized in stepwise fashion with a D-Tech 2000 alternating frequency (AF) demagnetizer, using peak fields progressively increasing on a logarithmically-spaced scale from 0.5 mT until the magnetization reached magnetometer noise levels (~10^{-11} Am^2). Remanence at each step was independently measured 30 times on each specimen using a 2G Enterprises superconducting quantum interference device magnetometer. Measurements with high noise/signal ratios were excluded from the calculation of the average values. Standard deviations were on the order of 1 nAm^2/kg. The characteristic remanence was isolated via principal component analysis (Kirschvink, 1980) using PuffinPlot (Lurcock and Wilson, 2012). We adopted the protocol devised by Peppe et al. (2009) for weak specimens, as follows: to define the characteristic remanence component we used either a) the best-fit line through a minimum of three consecutive demagnetization steps that trended toward the origin and had a maximum angular deviation (MAD) less than 20° (for specimens with quasi-linear trajectories, e.g., Figs. DR2, 2C-D), or b) a minimum of 4 consecutive demagnetization steps anchored to the origin, with MAD <20° (for specimens with directions clustering around one point, e.g., Fig. 2E). Because the speleothem is not azimuthally oriented, declination values were rotated so that average baseline values were situated in the interval [-10°, 30°], corresponding to realistic field declination values at the time in North America (e.g., Lund et al., 2005; Channell, 2006; Böhnel and Molina-Garza, 2002; Negrini et al., 2014). Mean declination was obtained by averaging adjusted declinations in the considered azimuthal interval at 1° increments. Virtual geomagnetic pole (VGP) coordinates were calculated at each adjusted declination step, and then combined to obtain mean and standard deviation values. After completing the NRM demagnetization, anhysteretic remanent magnetization (ARM) was imparted in the presence of a 0.05 mT bias field superimposed on an AF field decaying from a peak value of 100 mT, at a rate of 5 μT per half cycle. ARM susceptibility (χ_{ARM}) was calculated by normalizing the ARM to the bias field. Isothermal remanent magnetization (IRM) was imparted in a 1 T direct field using an impulse magnetizer. The ARM/IRM ratio (χ_{ARM}/IRM), computed by normalizing the ARM susceptibility by the IRM, is used as a magnetic grain size indicator, with higher values indicating finer bulk magnetic grain size.

Additional discrete (<500 mg) specimens from the speleothem were used for low temperature magnetic measurements to determine magnetic mineralogy. Low temperature saturation IRM was imparted in a 2.5 T field at 10 K following two separate treatments: field cooling in a 2.5 T field and zero-field cooling, from 300 to 10 K. Remanence behavior was then measured in zero field at 5 K intervals upon warming to room temperature. Finally, the behavior of a room temperature saturation IRM imparted in a 2.5 T field was measured in zero field at 5 K intervals while cooling the sample down to 10 K and then warming it back to 300 K.

REFERENCES CITED

Böhnel, H., and Molina-Garza, R., 2002, Secular variation in Mexico during the last 40,000 years: Physics of the Earth and Planetary Interiors, v. 133, p. 99–109.

Channell, J., 2006, Late Brunhes polarity excursions (Mono Lake, Laschamp, Iceland Basin and Pringle Falls) recorded at ODP Site 919 (Irminger Basin): Earth and Planetary Science Letters, v. 244, no. 1-2, p. 378–393, doi: 10.1016/j.epsl.2006.01.021.

Kirschvink, J.L., 1980, The least-squares line and plane and the analysis of paleomagnetic data: Geophysical Journal of the Royal Astronomical Society, v. 62, p. 699–718.

Lund, S.P., Scwartz, M., Keigwin, L., and Johnson, T., 2005, Deep-sea sediment records of the Laschamp geomagnetic field excursion (~41,000 calendar years before present): Journal of Geophysical Research, v. 110, B04101, doi: 10.1029/2003JB002943.

Lurcock, P.C., and Wilson, G.S., 2012, PuffinPlot: A versatile, user-friendly program for paleomagnetic analysis: Geochemistry, Geophysics, Geosystems, v. 13, no. 6, Q06Z45, doi: 10.1029/2012GC004098.

Negrini, R.M., McCuan, D.T., Horton, R.A., Lopez, J.D., Cassata, W.S., Channell, J.E.T., Verosub, K.L., Knott, J.R., Coe, R.S., Liddicoat, J.C., Lund, S.P., Benson, L. V, and Sarna-Wojcicki, A.M., 2014, Nongeocentric axial dipole field behavior during the Mono Lake excursion: Journal of Geophysical Research, v. 119, p. 2567–2581, doi: 10.1002/2013JB010846.

Peppe, D.J., Evans, D.A.D., and Smirnov, A.V., 2006, Magnetostratigraphy of the Ludlow Member of the Fort Union Formation (Lower Paleocene) in the Williston Basin, North Dakota: Geological Society of America Bulletin, v. preprint, no. 2008, p. 1, doi: 10.1130/B26353.1.

Table DR1. ^{230}Th dating results. The error is 2σ

Sample depth (mm)	^{238}U (ppb)		^{232}Th (ppt)		^{230}Th / ^{232}Th (atomic x10^{-6})		$\delta^{234}U$* (measured)		^{230}Th / ^{238}U (activity)		^{230}Th Age (yr) (uncorrected)		^{230}Th Age (yr) (corrected)		$\delta^{234}U_{Initial}$† (corrected)		^{230}Th Age (yr BP)§ (corrected)	
1.90 ±0.30	790	±1	18977	±380	612	±12	3507.5	±3.3	0.8925	±0.0015	23399	±48	23252	±115	3745	±4	23189	±115
13.45 ±0.25	688	±1	4537	±91	2921	±59	3079.8	±3.5	1.1679	±0.0022	35237	±82	35193	±87	3401	±4	35130	±87
23.00 ±0.50	778	±1	941	±19	16874	±342	2935.3	±4.3	1.2375	±0.0030	39250	±121	39242	±121	3279	±5	39179	±121
30.95 ±0.35	1003	±2	835	±17	24854	±504	2835.8	±3.9	1.2548	±0.0032	41102	±132	41096	±132	3184	±5	41033	±132
37.80 ±0.30	828	±1	489	±10	35313	±722	2780.2	±3.3	1.2656	±0.0024	42234	±101	42230	±101	3132	±4	42167	±101
49.40 ±0.30	772	±1	520	±11	31206	±639	2641.8	±2.8	1.2757	±0.0024	44560	±106	44556	±106	2996	±3	44493	±106
82.10 ±0.40	580	±1	1512	±30	8627	±174	2451.1	±2.8	1.3647	±0.0022	51538	±114	51518	±114	2835	±3	51455	±114
116.45 ±0.35	648	±1	5408	±108	2863	±58	2441.3	±3.5	1.4493	±0.0032	55650	±167	55587	±173	2856	±4	55524	±173
150.90 ±0.50	550	±1	36857	±739	365	±7	2308.2	±3.3	1.4856	±0.0032	60317	±181	59793	±412	2732	±5	59730	±412
185.80 ±0.80	449	±1	10149	±203	1157	±23	2335.8	±2.9	1.5854	±0.0031	64768	±177	64595	±215	2803	±4	64532	±215

U decay constants: λ_{238} = 1.55125x10^{-10} (Jaffey et al., 1971) and λ_{234} = 2.82206x10^{-6} (Cheng et al., 2013). Th decay constant: λ_{230} = 9.1705x10^{-6} (Cheng et al., 2013).

*$\delta^{234}U = ([^{234}U/^{238}U]_{activity} - 1)$x1000.

†$\delta^{234}U_{initial}$ was calculated based on ^{230}Th age (T), i.e., $\delta^{234}U_{initial} = \delta^{234}U_{measured} \times e^{\lambda_{234} \times T}$.

Corrected ^{230}Th ages assume the initial $^{230}Th/^{232}Th$ atomic ratio of 4.4 ±2.2 x10^{-6}. Those are the values for a material at secular equilibrium, with the bulk earth $^{232}Th/^{238}U$ value of 3.8. The errors are arbitrarily assumed to be 50%.

§B.P. stands for “Before Present” where the “Present” is defined as the year 1950 A.D.

Table DR2. Paleomagnetic and rock magnetic time series

Age (yr BP)	NRM (Am2/kg)	ARM (Am2/kg)	IRM (Am2/kg)	NRM/ARM	χ_{ARM}/IRM (mm/A)	Declination (degrees)	Inclination (degrees)	VGP Latitude (degrees)	VGP Latitude error (degrees)
23292	5.33E-07	2.56E-06	6.25E-05	0.207922	0.515064	28.26	52.67	66.6	10.7
27944.6	4.75E-08	8.34E-08	1.29E-06	0.569124	0.81343	19.49	49.38	71.3	9.3
33114.1	1.42E-07	2.70E-07	6.42E-06	0.524644	0.529256	30.46	53.68	65.2	10.7
36423.2	8.23E-08	1.69E-07	2.82E-06	0.487076	0.75422	-15.56	46.81	72	7.9
38542.9	8.45E-08	9.81E-08	2.35E-06	0.862019	0.524338	34.17	65.11	63.2	9.1
39995	1.13E-08	3.68E-08	5.01E-07	0.306445	0.922701	84.89	30.47	14	10.6
41103.1	3.73E-09	4.71E-08	4.73E-07	0.0791692	1.25149	133.79	11.32	-28.3	8.8
41910.1	5.23E-09	2.96E-08	4.21E-07	0.176279	0.884015	28.23	9.82	47.3	7.4
42858.4	2.79E-08	4.47E-08	5.58E-07	0.62411	1.00707	12.99	56.03	78	8.8
43845.9	1.66E-08	3.85E-08	5.42E-07	0.430773	0.892482	-4.87	57.31	80.8	6.2
44843.8	2.33E-08	4.75E-08	8.09E-07	0.490018	0.737676	67.55	66.02	41.3	8.8
45897.7	5.00E-08	6.30E-08	9.53E-07	0.793532	0.831496	10.50	75.71	62.9	2.1
46941	3.51E-08	6.10E-08	1.64E-06	0.576282	0.465807	33.40	29.22	52.5	9.2
47973.6	4.29E-08	5.99E-08	1.10E-06	0.715997	0.682593	4.97	53.26	79.3	5.5
49016.9	3.09E-08	6.95E-08	1.09E-06	0.444806	0.802337	4.76	43.75	73.6	4
50070.8	3.19E-08	5.24E-08	8.62E-07	0.608729	0.763337	19.49	46.98	70	8.9
51124.8	3.62E-08	1.07E-07	1.37E-06	0.33816	0.980018	-18.46	53.65	74	9.9
51833.8	2.75E-08	4.14E-08	8.18E-07	0.664378	0.635575	13.16	74.37	64.4	2.9
52402.5	4.26E-08	6.41E-08	7.80E-07	0.664964	1.03262	17.99	69.03	69.4	5.6
52988.8	1.59E-07	2.20E-07	4.79E-06	0.722937	0.576672	0.00	47.33	76.2	3.7
53584.1	2.03E-07	3.06E-07	8.19E-06	0.66483	0.469031	-1.36	50.51	78.2	4.3
54170.5	7.73E-08	1.60E-07	2.63E-06	0.483591	0.762092	9.07	56.13	79.5	7.4
54742.1	1.53E-07	3.63E-07	6.29E-06	0.421753	0.726309	35.50	56.02	61.9	10.7
55322.5	1.52E-07	2.27E-07	5.05E-06	0.668087	0.56533	11.71	36.99	67.8	5.5
55908.5	1.54E-07	2.01E-07	6.96E-06	0.766462	0.361779	-13.45	31.26	64	5.5
56494.6	2.60E-07	4.25E-07	1.76E-05	0.6121	0.30387	-12.93	35.84	66.7	5.7
57099	4.21E-07	7.48E-07	3.20E-05	0.563701	0.293534	-11.50	52.44	77	7.6
57691.2	8.23E-07	2.43E-06	0.00012813	0.338623	0.238231	-2.55	57.84	81	5.4
58283.3	7.06E-07	1.98E-06	0.00012026	0.35683	0.206741	11.93	55.31	78.2	8.3
58878.6	3.56E-07	1.19E-06	5.83E-05	0.298329	0.257438	-9.26	65.56	75.4	4.8
59437.1	3.13E-07	1.24E-06	6.88E-05	0.252824	0.225952	12.31	33.21	65.4	5.3
60057	6.65E-07	2.36E-06	0.00013179	0.28189	0.225067	-16.21	45.98	71.2	7.9
60769	6.73E-07	1.02E-06	5.44E-05	0.65775	0.23625	34.71	58.18	63	10.5
61477.7	4.66E-07	1.20E-06	6.84E-05	0.388535	0.220435	24.26	41.07	64	9.1
62172.5	2.96E-07	6.18E-07	2.78E-05	0.478151	0.279665	0.44	38.51	70.7	2.9
62888.1	3.04E-07	7.64E-07	3.37E-05	0.398166	0.284751	-10.61	39.09	69.4	5.4
63596.7	3.51E-07	1.03E-06	4.18E-05	0.339652	0.311065	12.76	47.12	73.4	7
64284.7	1.64E-07	9.09E-07	3.12E-05	0.180789	0.366401	5.28	58.74	80.5	5.9

Table DR3. Incremental chronology

Depth (mm)	Age (yrs BP)	Growth rate (mm/kyr)
22.500	39192	4.24
22.623	39221	4.24
22.777	39266	3.41
23.187	39392	3.25
23.316	39434	3.07
23.592	39551	2.37
23.623	39564	2.37
24.053	39742	2.42
24.178	39763	5.95
24.368	39813	3.80
24.436	39833	3.37
24.475	39847	2.80
24.542	39870	2.91
24.624	39894	3.40
24.690	39909	4.43
24.725	39917	4.41
24.976	39977	4.18
25.188	40017	5.29
25.366	40048	5.76
25.408	40057	4.67
25.654	40109	4.73
25.858	40156	4.34
26.116	40214	4.44
26.203	40229	5.82
26.267	40242	4.96
26.380	40261	5.91
26.503	40281	6.18
26.762	40331	5.18
26.977	40373	5.11
27.201	40417	5.09
27.270	40432	4.62
27.492	40466	6.51
27.563	40482	4.45
27.801	40523	5.80
27.896	40552	3.29
27.986	40569	5.26
28.198	40611	5.05
28.312	40630	6.00
28.442	40646	8.16
28.614	40677	5.52
28.708	40694	5.54
28.788	40708	5.70
28.902	40728	5.71
29.083	40757	6.26
29.168	40770	6.54
29.522	40812	8.41
29.772	40849	6.78
29.859	40863	6.21
30.312	40917	8.38
30.410	40928	8.91
30.724	40964	8.72
30.860	41001	3.68
30.952	41014	7.10
31.149	41040	7.56
31.423	41076	7.63
31.448	41081	5.00
31.669	41116	6.32
31.771	41131	6.78
32.016	41166	7.00
32.282	41209	6.19
32.368	41223	6.16
32.578	41258	5.99
32.648	41270	5.85
32.740	41287	5.37
32.922	41318	5.87
33.086	41348	5.48
33.460	41408	6.23
33.767	41452	6.98
33.963	41485	5.95
34.192	41522	6.18
34.359	41547	6.66
34.610	41592	5.59
34.688	41608	4.84
34.760	41624	4.52
34.793	41631	4.75
34.898	41652	4.96
34.977	41668	4.94
35.281	41716	6.34
35.503	41747	7.15
35.607	41767	5.22
36.266	41869	6.46
36.410	41889	7.16
36.478	41900	6.20
36.573	41917	5.62
37.191	42013	6.43
37.623	42084	6.08
37.766	42111	5.30
38.100	42167	5.97

Fig. DR1. Confocal micrograph showing fluorescent annual layering in the studied speleothem.

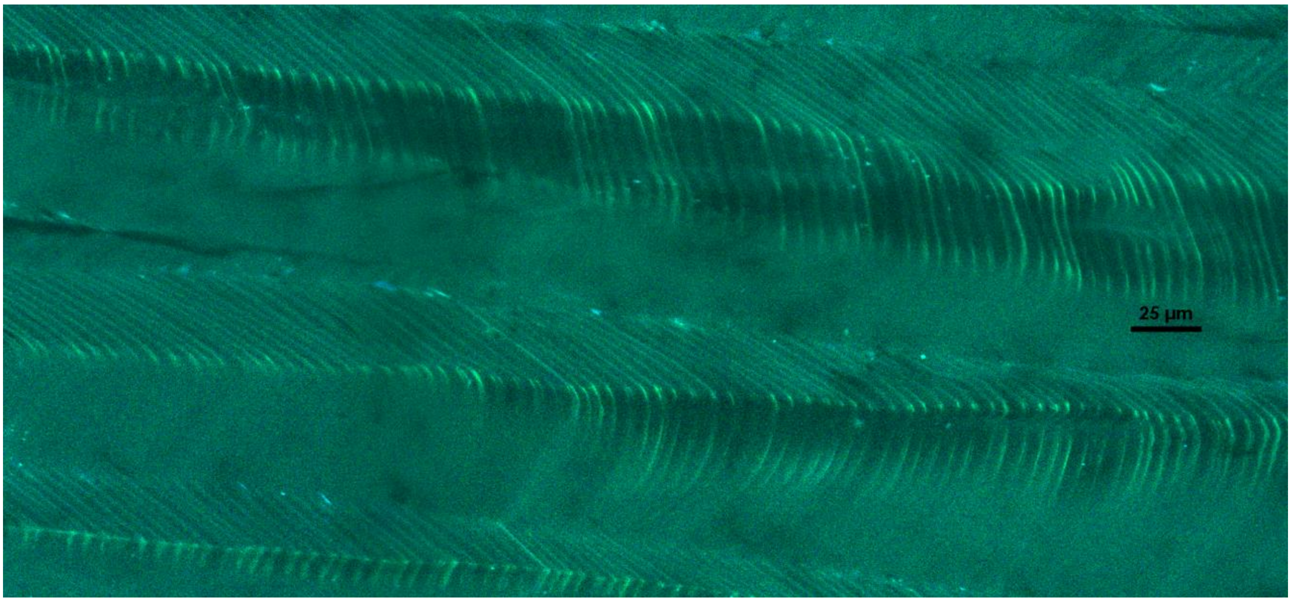

Fig. DR2. Orthogonal projection and azimuthal equidistant plot of the specimen from 62 ka BP. Full (open) squares represent the horizontal (vertical) projections of the demagnetization vectors (grey arrows). Magnetometer noise level is $\sim 10^{-11}$ Am^2.